Proceedings of
10th European Conference on Turbomachinery Fluid dynamics & Thermodynamics
ETC10, April 15-19, 2013, Lappeenranta, Finland

STUDY ON THE EFFECTS OF AXIAL CLEARANCE SIZE ON THE OPERATION OF AN AXIAL FLOW ELECTRIC MOTOR COOLING FAN

J. Vad – Cs. Horváth

Department of Fluid Mechanics, Budapest University of Technology and Economics (**BME**)
Bertalan Lajos u. 4 - 6., H-1111 Budapest, Hungary. Email: vad@ara.bme.hu

ABSTRACT

In the case of axial flow fan rotors used for electric motor cooling, an axial clearance is present between the rotor shroud inlet and the perforated cover. The effect of axial clearance size on the operation of a case study fan has been investigated. The means of investigation were Computational Fluid Dynamics (CFD) and Computational Aero-Acoustics (CAA). The CFD and CAA results revealed that the axial clearance size is a sensitive parameter in influencing both fan aerodynamics and aero-acoustics, for which the major mechanisms, associated with the leakage flow, were qualitatively identified. The studies suggested the existence of an acoustically unfavourable clearance size for which maximum noise emission can be expected. A semi-empirical model was outlined as a starting point in prediction of cooling flow rate as a function of axial clearance size as well as other parameters.

NOMENCLATURE

c_x	[m]	axial clearance between the shroud inlet plane and the perforated cover
C_C	[-]	coefficient of contraction
d_t	[m]	blade tip diameter
k	[$(m/s)^2$]	turbulent kinetic energy
L_W	[dB]	acoustic power level
Ma	[-]	tip Mach number: u_t divided by speed of sound in air at 20 °C
N	[-]	blade count
p	[Pa]	static pressure
Δp_L	[Pa]	pressure difference driving the leakage flow
Δp_R	[Pa]	difference of mass-averaged static pressures downstream and upstream of the rotor
Δp_ω	[Pa]	static pressure difference through the clearance in radial direction, due to rotation
ΔR	[m]	radial extension of clearance
Re	[-]	Reynolds number: $u_t \cdot d_t$ divided by air kinematic viscosity at 20 °C
u_t	[m/s]	blade tip circumferential velocity
v	[m/s]	absolute velocity
v_L	[m/s]	leakage flow velocity
v_u	[m/s]	tangential component of absolute velocity
y^+	[-]	wall normal cell size (in wall units)
ν	[-]	hub-to-tip diameter ratio
ρ	[kg/m^3]	fluid density
Φ	[-]	flow coefficient: volume flow rate / (u_t·annulus area)
Ψ	[-]	total pressure rise coefficient: mass-averaged total pressure rise / ($\rho \cdot u_t^2/2$)
$\Delta\Psi_R$	[-]	rotor static pressure difference coefficient: Δp_R / ($\rho \cdot u_t^2/2$)
ω	[1/s]	angular speed of the rotor

SUBSCRIPTS

C cooling flow rate: delivered toward the cooling ribs
L leakage flow rate: leaking back through the axial clearance
mean mean value in the clearance
R rotor flow rate: flowing through the rotor
0 reference condition obtained in CFD simulation for zero axial clearance

1. INTRODUCTION

In electric motor cooling, replacing radial fan rotors with axial fan rotors offers a potential for reduction of fan noise and absorbed fan power while retaining the demanded cooling performance, as demonstrated in the case study by Vad et al. (2011), and outlined by Borges (2012). The photo of the axial rotor studied in the present paper, together with the sketch on the typical flow path, is presented in **Figure 1**. The air enters the fan via a perforated front cover, directing the airflow towards the cooling ribs located at the motor periphery. The air enters the rotor nearly axially, and is diverted radially outward. The installation of an electric motor cooling fan, due to the presence of the front cover, is unusual from the point of view of aerodynamics and aero-acoustics of industrial axial fans. Rotors of industrial axial fans, often incorporated in a ducted configuration, are characterised by a *radial* clearance between the blade tip and the casing wall. The effects near the blade tip of the fan rotor, exhibiting a radial clearance, have been subject of extensive research (e.g. Bianchi et al., 2011). Nevertheless, the axial rotors applied for cooling of electric motors are shrouded, and an *axial* clearance is present between the perforated inlet cover and the rotor. Such axial clearance has been found to have a significant impact on fan aerodynamics and aero-acoustics (Vad et al., 2011). To the authors' best knowledge, the effect of axial clearance in electric motor cooling fans has not been studied so far by others. The results of extensive research related to axial flow automotive cooling fans (e.g. Verstraete et al., 2011; Zayani et al., 2012) cannot be fully adapted to electric motor cooling fans, due to the geometrical differences in the confined rotor environment.

As continuation to the work documented in Vad et al. (2011), the present paper aims at providing novel information on axial clearance effects, contributing to prediction of fan aerodynamic and acoustic performance in preliminary design. The means of investigation is a validated Computational Fluid Dynamics (**CFD**) tool, coupled with Computational Aero-Acoustics (**CAA**) simulation. Basic fluid mechanical considerations are also involved while elaborating a semi-empirical model for prediction of leakage flow rate through the axial clearance.

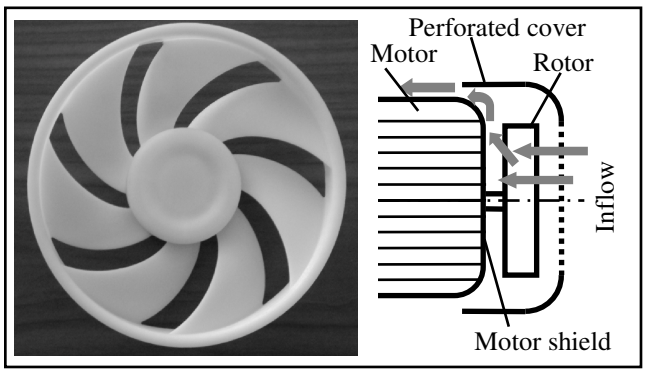

Figure 1. Photo of the axial flow rotor, and simplified meridional scheme of flow path (reproduced from Vad et al., 2011)

2. AXIAL ROTOR OF CASE STUDY

The rotor (Fig. 1) has been designed using a controlled vortex design concept as outlined in Vad et al. (2011). It incorporates circumferentially forward-skewed blades. Data on the rotor, confined to dimensionless global characteristics for confidentiality reasons, are presented in **Table 1**. The rotor environment can be overviewed in the following figures, and in Vad et al. (2011).

The operation of the rotor has been investigated for four axial clearance sizes of c_x/d_t = 0 % (zero clearance), 1.29 %, 2.54 %, and 3.79 %. The CFD and CAA plots shown in the following sections present the four investigated cases, in the sequence of axial clearance increasing from the left to the right.

Table 1. Rotor characteristics

N	7	ν	0.403
Re	$1.47 \cdot 10^5$	Φ_0	0.139
Ma	$5.17 \cdot 10^{-2}$	Ψ_0	0.364

3. CFD AND CAA TECHNIQUE

Steady flow simulations were carried out using the commercially available finite-volume CFD code ANSYS 13.0 Fluent (2010). The k-ω SST model was applied, on the basis of past experiences (Vad et al., 2011). Fully turbulent flow was assumed, with no transitional models being applied. Sensitivity studies were carried out in setting the size of the blow-out zone volume to various sizes. In the applied CFD domain, independence from the blow-out zone size has been achieved. At the sides of the blow-out zone, the boundary condition was "pressure-outlet". **Figure 2** presents the computational domain. Taking periodicity into consideration, the computations regarded only one blade pitch. Utilizing the features of the annular cascade configuration, boundary conditions of periodicity were applied. The inlet face is a sector of a virtual cylindrical inlet pipe (see Vad et al., 2011 for explanation) with a central angle of 360°/N. Downstream of the inlet face, sectors of the fan cover and the rotating hub, with one blade in the middle of the domain, are included. At the inlet face, located upstream of the fan casing, within the suction pipe, a steady pressure inlet is defined. The inlet turbulence intensity has been set to 10 % and the hydraulic diameter was set to the diameter of the virtual cylindrical inlet pipe, in order to reproduce former experimental experiences. The perforated casing is reproduced using a porous material. Approximately 50 % of the cells are located in the refined domain in the vicinity of the blade. The computational domain embedding the rotor was composed from meshes of two different type, in order to achieve the best grid quality with a fast mesh generation process. A proper block structured mesh was generated around the blade O-grid. On the shroud and hub faces, boundary layer meshes were applied. ANSYS BladeGen and ANSYS TurboGrid were used to generate and mesh the adjacent domains of the blade. The quality of the mesh was checked using the built-in checker of ANSYS TurboGrid and by means of validation calculations.. The mesh in the blade passage domain – termed "passage-domain mesh" was created only once, and, using ANSYS Fluent non-conformal interfaces (ANSYS 13.0 Fluent (2010)), was connected to the mesh of the surrounding domain of each case. The geometry of the surrounding domain was based on the passage-domain mesh and was extrapolated from it. A proper block structured mesh was generated with the aid of H-type boundary and shear layer mesh resolution. Four geometries were developed with different axial clearance sizes by means of ANSYS ICEM. A good mesh quality and the adequate positioning of the interfaces were basic requirements. The skewness of the cells in the surrounding domains was below 0.8. The volume change and aspect ratios also confirmed the good quality of the mesh. The mesh can be characterized by a value of $y^+ < 3$ and an orthogonal quality greater than 0.25. At the non-conformal interfaces, the cell sizes were synchronized. The interfaces were planar faces and were placed as far

as possible from the observed areas. The two non-continuous meshes were connected numerically with the aid of the non-conformal interfaces. A multiple reference frame model was used during the simulations in modelling the rotation of the moving walls. Typical computations required approximately 14,000-17,000 iterations. The solutions were considered converged when the scaled residuals of all equations were resolved below the levels of order of magnitude of 10^{-3} and the surface monitors remained practically constant. Journal files were used in automating the calculations. The speed of revolution of the moving walls was gradually increased to the operational speed, and then the porous zones representing the perforated fan cover and the cooling ribs were switched on.

For CFD validation, the computed cooling flow rate – i.e. flow rate delivered toward the cooling ribs, being equal to the inlet flow rate through the perforation of the front cover –, being dependent on the axial clearance size, was compared to experimental data reported in Vad et al. (2011). The computed and measured cooling flow rate values are presented in **Figure 3a)**. The error bars correspond to the experimental uncertainty. The fair quantitative agreement between the CFD and experimental data, along with the proper resolution of the trend of decreasing flow rate with increasing clearance size support the validity of the CFD tool.

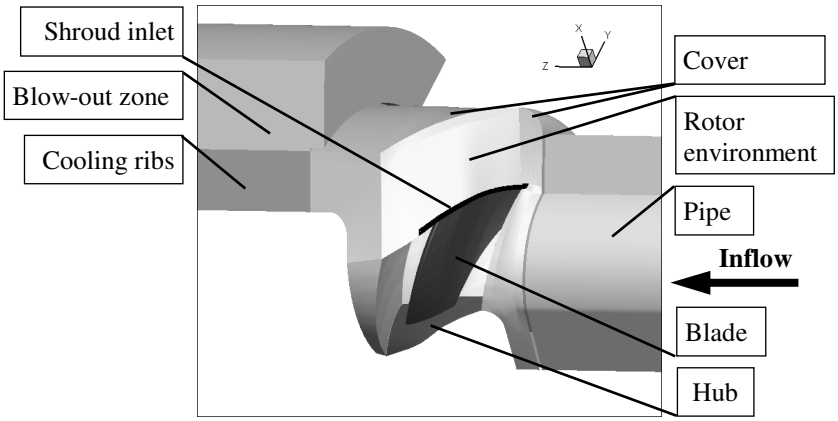

Figure 2. Details of computational domain

For obtaining qualitative acoustic information on the effect of axial clearance size, ANSYS CAA tools for localizing broadband noise sources, which are based on the steady CFD results, and which have already been applied in Horváth and Vad (2009), have been used. The acoustic source terms on the walls have been estimated on the basis of boundary layer parameters, as well as in the free shear layers. The application of this CAA methodology to industrial axial fans has been inspired e.g. by Cros and Carbonneau (2009).

4. RESULTS AND DISCUSSION

Figure 4 presents the plots of computed absolute velocity magnitude and acoustic power level over a planar inlet section of the computational domain. The interrogation plane is perpendicular to the axis of rotation, and is located at the entrance of the cylindrical inner surface of the shroud, downstream of the rounded inlet rim of the shroud. The arch-shaped white zone in the plots corresponds to the cross-section of the shroud. At zero clearance, the interrogation plane coincides with the inner surface of the cover at the lowest and the highest radii, and therefore, no computational data are presented for these regions. The figure demonstrates that the leakage velocity peak and leakage flow rate become higher as the axial clearance increases (upper row). The turbulent leakage jet appears as a dominant source of noise in the interrogation plane (lower row).

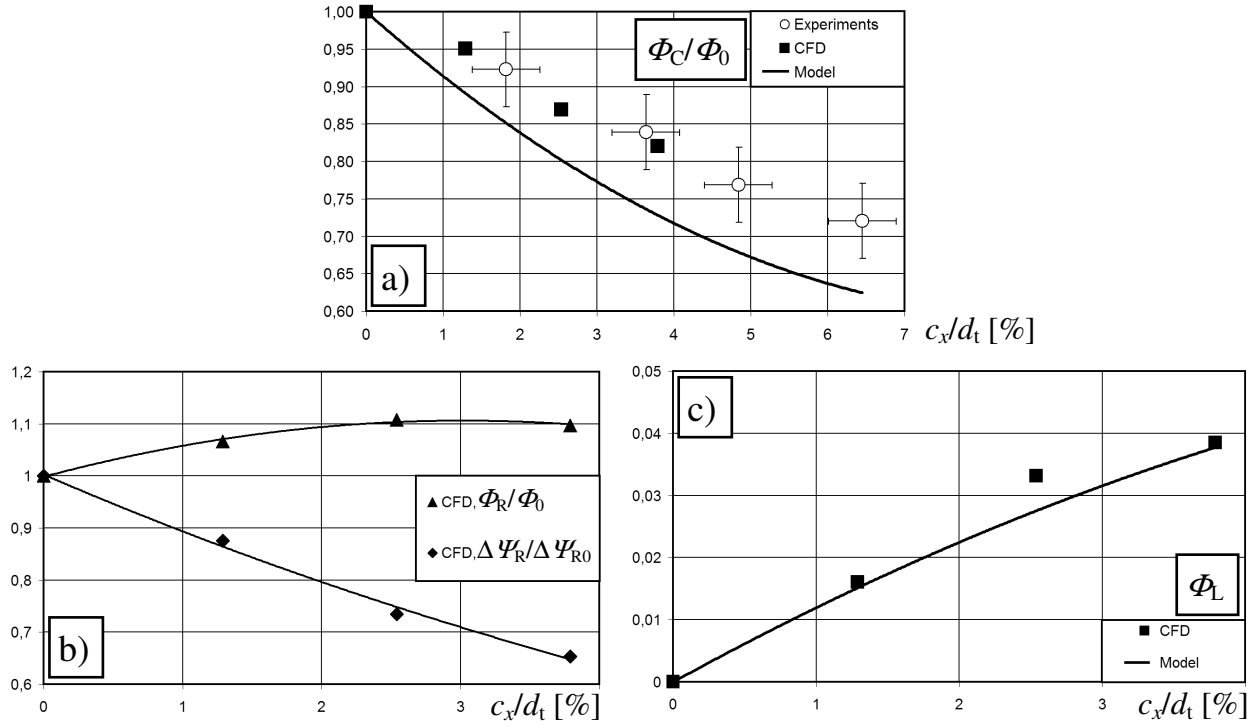

Figure 3. Trends due to change of axial clearance size. a) Measured, computed and semi-empirically modelled cooling flow rate. b) Computed rotor flow rate and pressure difference. c) Computed and semi-empirically modelled leakage flow rate.

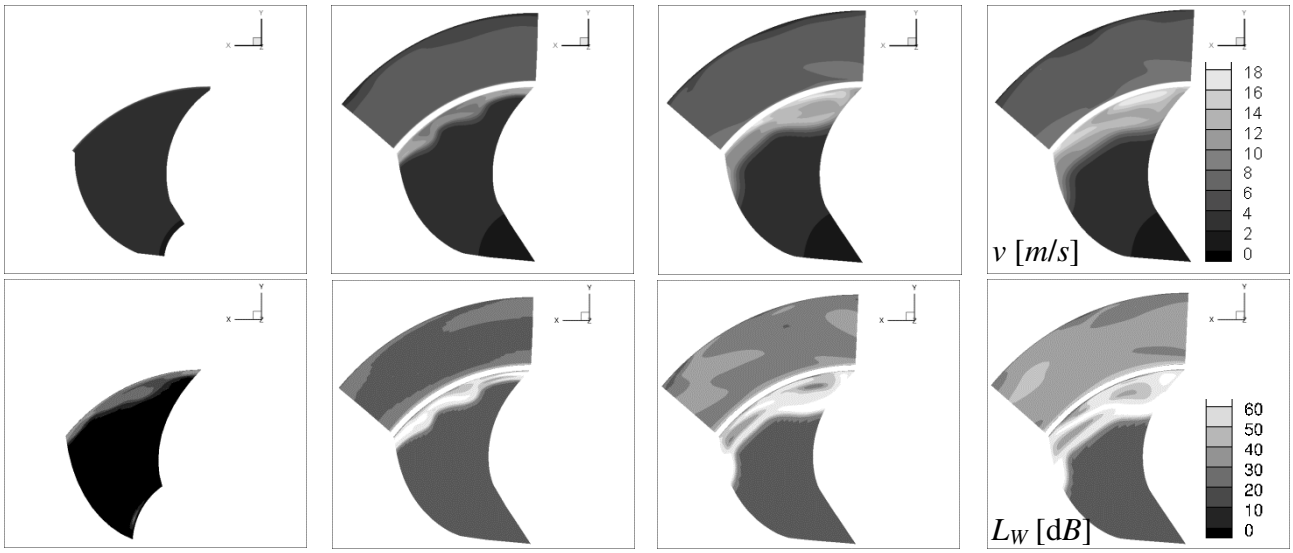

Figure 4. Viewing the inlet section of computed domain from axial direction. Axial tip clearance increasing from the left to the right. Upper row: magnitude of absolute velocity. Lower row: acoustic power level.

A more comprehensive explanation can be given on the clearance-related phenomena with use of the absolute tangential velocity, turbulent kinetic energy, and acoustic power level plots over a longitudinal section, using **Figure 5**. The interrogation plane fits the axis of rotation and intersects the blade near the tip leading edge (the blade is viewed in the figure). The upper limit of the scale of the tangential velocity (white color) corresponds to u_t. The inlet fluid flowing nearly axially through

the perforated cover interacts with the rotating inlet rim of the shroud. The tangential velocity plots (uppermost row) reveal that this interaction results in a rotating separation zone. The nearly radially inward leakage flow tends to intensify the detachment of flow from the inlet rim of the shroud. The larger the clearance – i.e. the more intense the leakage flow –, the more extended the rotating separation zone, and the higher the magnitude of rotation. At the largest clearance, the k plot (fourth plot in the middle row) demonstrates the presence of two separate zones of high turbulence past the clearance: i) The shear layer at the interaction between the leakage flow and the inlet flow through the cover, ii) The rotating separation zone, bounded by the leakage flow. As the clearance size decreases, these two zones tend to get closer, and, at a certain clearance size, they are merged. This mergence phenomenon results in extremely high local k values, and, accordingly, an absolute maximum in the local acoustic power level (second plots in the middle and lowermost rows). Although Fig. 4 suggests that the leakage flow noise tends to intensify with increasing clearance size, the lowermost row in Fig. 5 draws the attention that this trend is not obviously monotonous: loci of absolute maximum of sound power are present in the plots of intermediate clearance sizes.

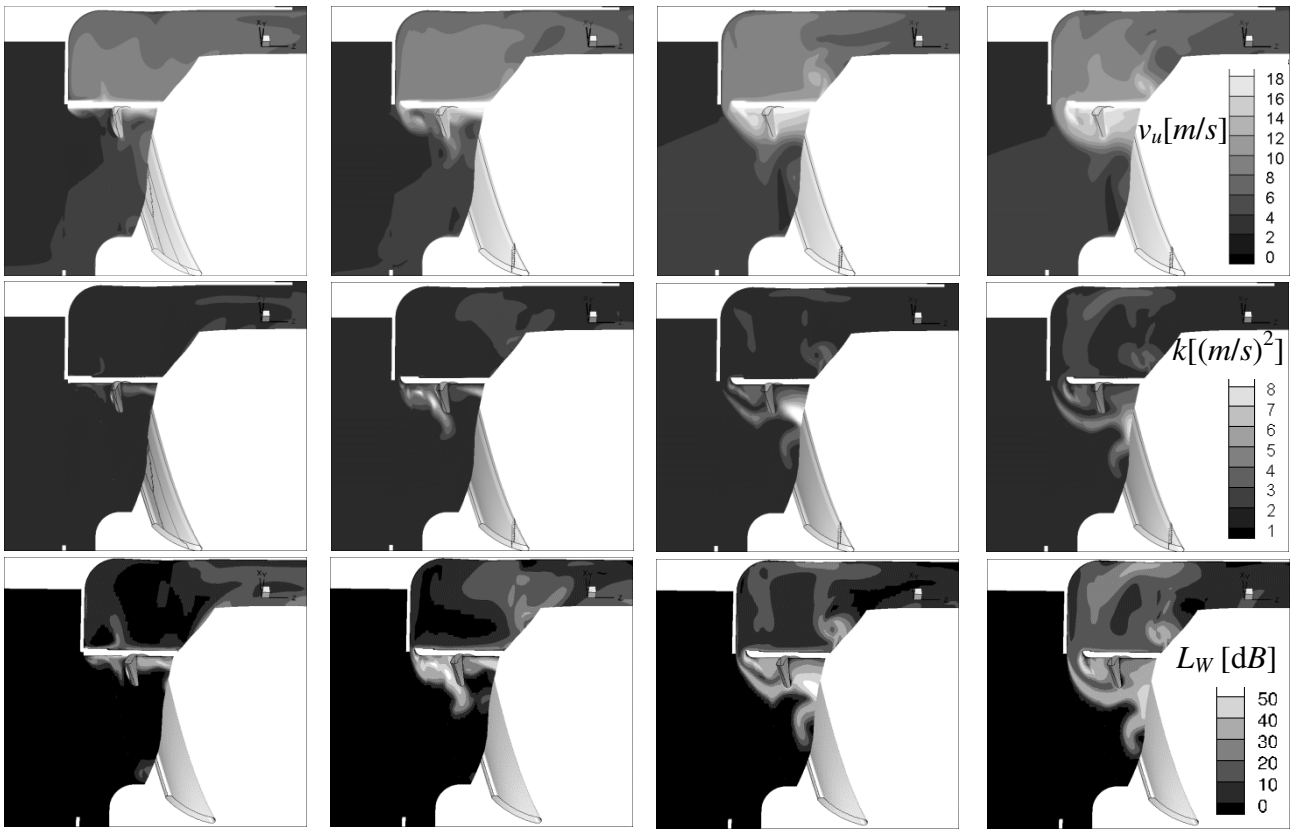

Figure 5. Longitudinal section of computed domain. Axial tip clearance increasing from the left to the right. Upper row: tangential component of absolute velocity. Middle row: turbulent kinetic energy. Lower row: acoustic power level.

The impact of the near-clearance phenomena on blade aerodynamics and blade acoustics can be viewed in **Figures 6 and 7**. In Fig. 6, the static pressure over the blade pressure surface is plotted. According to the presence of the rotating separation zone upstream of the blade leading edge, the incidence angle of the relative flow to the blade decreases, and so does the blade load. This results in reduced static pressure values near the leading edge on the pressure side, in the radial region where the rotating separation zone affects the flow incidence. The larger the clearance size, the more the pressure reduction near the leading edge – due to a more pronounced effect of the rotating separation zone –, and the more the extension of the low-pressure region toward lower radii.

In Fig. 7, the static pressure as well as the acoustic power level over the blade suction surface is presented. The blade unloading effect due to the rotating separation zone, affected by the clearance size, is also visible here in the static pressure diagrams. At zero clearance (upper row, first plot), a pronounced suction effect is visible near the leading edge, followed by an adverse pressure gradient as one moves toward the trailing edge. In the suction side blade tip-shroud corner, near the leading edge, a zone of nearly constant static pressure can be detected. This suggests the presence of a separation zone that is probably due to local blade overloading caused by the negative dihedral (Vad, 2008). Increasing the clearance, the suction effect and the adverse pressure gradient, manifesting the blade load, tend to decrease, and tend to confine to lower radii. As seen in the acoustic power level plot for zero clearance (lower row, first plot), the separation zone near the tip leading edge appears as a source of peak noise. As the clearance increases, the leakage flow tends to energize the separation zone. As a result, the noise associated with the separation zone moderates. The zone of highest acoustic power level tends to distribute toward lower radii, with lower values of maximum surface acoustic power level.

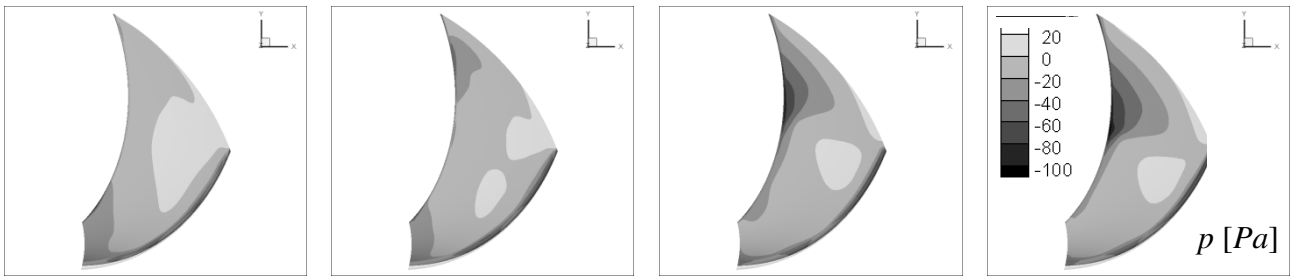

Figure 6. Blade pressure surface. Axial tip clearance increasing from the left to the right. Static pressure.

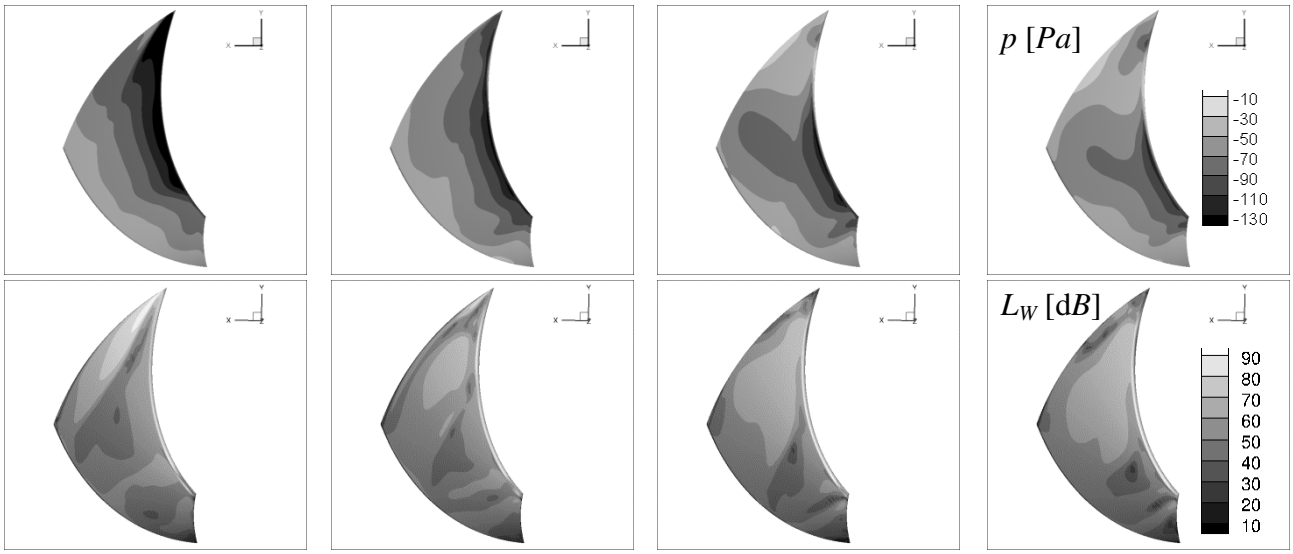

Figure 7. Blade suction surface. Axial tip clearance increasing from the left to the right. Upper row: static pressure. Lower row: surface acoustic power level.

The observations related to the acoustic power level plots in Figs. 4, 5 and 7 suggest the existence of an acoustically unfavourable intermediate clearance size for which maximum noise emission can be expected. This topic is a subject of further studies, also involving acoustic measurements.

5. SEMI-EMPIRICAL MODEL FOR FLOW RATE PREDICTION

A semi-empirical model is intended to be developed for prediction of volumetric loss associated with the leakage flow – i.e. leakage flow rate –, and for prediction of effective cooling flow rate. A preliminary version of the model is documented herein. In its final form, the model will contribute to performance prediction in design of axial fans used for electric motor cooling.

Δp_R is the difference between mass-averaged static pressures downstream and upstream of the rotor. According to the blade unloading effect discussed using Figs. 6 and 7, Δp_R is expected to decrease with increasing clearance. This trend can be observed in the CFD-based $\Delta \Psi_R / \Delta \Psi_{R0}$ plots in **Figure 3b)**. An exponential trend line fits the data points well, as presented in the figure. The related exponential function is used in further modelling, fulfilling the asymptotic condition of $\Delta p_R \to 0$ if $c_x/d_t \to \infty$.

The fluid rotates in the clearance. The front wall of the clearance, i.e. the cover, is motionless. The rear wall of the clearance, i.e. the inlet rim of the shroud, rotates at an angular speed ω. As a first approximation, it has been assumed that the fluid in the clearance rotates at a mean angular speed of $\omega_{mean} = \omega/2$. A radial pressure gradient develops in the clearance. The resultant pressure difference Δp_ω acts against Δp_R in driving the leakage flow. Δp_ω is expressed from the following approximate relationship, based on the radial component of Euler equation:

$$\frac{\partial p}{\partial n} = \frac{\Delta p_\omega}{\Delta R} = \rho \frac{v_{u\,mean}^2}{R_{mean}} = \rho R_{mean} \omega_{mean}^2 = \rho \left(\frac{d_t}{2} + \frac{\Delta R}{2} \right) \left(\frac{\omega}{2} \right)^2 \tag{1}$$

The pressure difference driving the leakage flow is as follows:

$$\Delta p_L = \Delta p_R - \Delta p_\omega \tag{2}$$

It is assumed on the basis of the Bernoulli equation that a leakage flow of velocity v_L develops through the clearance:

$$v_L = \sqrt{\frac{2 \Delta p_L}{\rho}} \tag{3}$$

It can be shown that the hydraulically equivalent diameter of the clearance – taken as 4 times the mean cross-section in the clearance divided by the wetted circumference (over the two peripheries of the clearance) – is 2 c_x.

The leakage flow is contracted in the clearance. The contraction coefficient C_C, being dependent on 2 c_x and ΔR (i.e. diameter and length of a hydraulically equivalent cylindrical Borda mouthpiece) is approximated on the basis of Dong and Lienhard (1986).

The leakage flow rate is predicted as follows:

$$q_L = 2 R_{mean} \pi c_x C_C v_L \tag{4}$$

Figure 3c) makes a comparison between the leakage flow rate data supplied by the CFD tool as well as predicted using the semi-empirical model ("Model" in the figure). Despite the simplifying assumptions made in the model, a fair agreement is observable.

The cooling flow rate is then to be calculated as

$$q_C = q_R - q_L \tag{5}$$

Where q_R is the actual flow rate through the rotor. As the diagram in Fig. 3b) shows, q_R varies with the clearance size. At this preliminary state of modelling, q_R is taken briefly as $q_R \equiv q_0$. This implies, considering Eq. (5), the following approximation:

$$q_C = q_0 - q_L \tag{6}$$

The semi-empirically modelled cooling flow rate is presented in Fig. 3a) ("Model" in the figure). Although the trend of flow rate decrease is fairly well represented by the model, it gives a conservative (pessimistic) estimation on the cooling flow rate: the data obtained from the model are below the measured ones. The following ways of improving the model are envisaged, in the sequence of anticipated importance: i) Semi-empirical modelling of q_R, instead of the approximation of $q_R \equiv q_0$, in Eq. (5) (conf. Fig. 3b)). ii) A more accurate consideration of C_C in Eq. (4). iii) An appropriate extension of Bernoulli equation, represented in Eq. (3), to friction losses, e.g. loss at inlet to the clearance. iv) A more accurate consideration of effect of rotation in the clearance, instead of the approximation of $\omega_{mean} = \omega/2$ in Eq. (1). The model improvement is to be based on further CFD studies, focussing on the aforementioned details.

5. SUMMARY

The CFD and CAA studies as well as theoretical considerations lead to the following novel results in surveillance of effect of axial clearance size on the operation of a case study axial flow rotor used in electric motor cooling.

1) The following comprehensive explanation has been given on the mechanisms via which the size of axial clearance size affects the fan aerodynamic performance. The fluid entering via the perforated cover interacts with the rotating inlet rim of the shroud. This results in a rotating separation zone. The inward leakage flow tends to intensify the detachment of flow from the rim. The rotating separation zone causes a moderation in flow incidence angle to the blades, and thus, a moderation in blade load and in pressure rise occurs. The more the axial clearance size, i) the more intense the leakage flow rate, ii) the higher the rotation and larger the extension of the rotating separation zone, iii) the more pronounced the effect of deteriorating the flow incidence to the blades, the blade load, and the pressure rise.

2) The leakage flow-related noise generation phenomena were investigated, such as i) noise of the turbulent leakage flow, being intensified with axial clearance size, ii) possible mergence of high-turbulence regions (shear layer at the inlet, rotating separation zone), apparently causing a maximum in the local acoustic power level at an intermediate clearance size, iii) noise related to a separation zone in the blade tip-shroud corner over the suction surface, being attenuated with axial clearance size. These observations suggest the existence of an acoustically unfavourable intermediate clearance size for which maximum noise emission can be expected. This topic is a subject of further study.

3) A preliminary version of a semi-empirical model has been elaborated, with the aid of the CFD studies, for prediction of clearance size-dependent flow rate. The model fairly well predicts the leakage flow rate. The model provides a conservative (pessimistic) prediction on the effective cooling flow rate. The way for further developing the model has been outlined.

ACKNOWLEDGEMENTS

The paper has been supported by the Hungarian National Fund for Science and Research under contract K 83807. Gratitude is expressed to Mr. Gábor Kiss for assisting the CFD studies, as well as to Mr. Richárd Budafoki and Mr. László Vitai giving assistance in developing the semi-empirical model.

REFERENCES

Bianchi, S., Corsini, A., Sheard, A. G. (2011), Experimental aero-acoustic characterization of axial fan fitted with shaped tip end-plates. *Proc. 9th European Conference on Turbomachinery Fluid Dynamics and Thermodynamics (ETC'9)*, Istanbul, Turkey, pp. 1653-1663.

Borges, S. S. (2012), CFD techniques applied to axial fans design of electric motors. *Proc. International Conference on Fan Noise, Technology and Numerical Methods (FAN2012)*, Senlis, France (CD-ROM, ISBN 978-0-9572374-1-4)

Cros, S., Carbonneau, X. (2009), *Computational study of the aerodynamic impact of stall margin improvements in a high tip speed fan.* Proc. 8th European Conference on Turbomachinery Fluid Dynamics and Thermodynamics (ETC'08), Graz, Austria, pp. 401-410.

ANSYS 13.0 Fluent User's guide (2010) (ANSYS, Inc., Canonsburg, PA, USA)

Dong, W.-g., Lienhard, J. H. (1986), *Contraction coefficients for Borda mouthpieces*. ASME J. Fluids Engineering, **108**, pp. 377-379.

Horváth, Cs., Vad, J. (2009), *Broadband noise source model acoustical investigation on unskewed and skewed axial flow fan rotor cascades.* Proc. Conference on Modelling Fluid Flow (CMFF'09), Budapest, Hungary, pp. 682-689.

Vad, J. (2008), *Aerodynamic effects of blade sweep and skew in low-speed axial flow rotors at the design flow rate: an overview.* Proc. Inst Mech Engineers – Part A: J. Power and Energy, **222**, pp. 69-85.

Vad, J., Horváth, Cs., Lohász, M. M., Jesch, D., Molnár, L., Koscsó, G., Nagy, L., Dániel, I., Gulyás, A. (2011), Redesign of an electric motor cooling fan for reduction of fan noise and absorbed power. *Proc. 9th European Conference on Turbomachinery Fluid Dynamics and Thermodynamics (ETC'9)*, Istanbul, Turkey, pp. 69-79.

Verstraete, T., Roytta, P., Henner, M., Alsalihi, Z., Brouckaert, J. F. (2011), Design and off-design optimization of a fan for automotive applications. *Proc. 9th European Conference on Turbomachinery Fluid Dynamics and Thermodynamics (ETC'9)*, Istanbul, Turkey, pp. 1485-1496.

Zayani, M., Cağlar, Ş., Gabi, M. (2012), Aeroacoustical investigations on axial fans for automotive cooling systems. *Proc. International Conference on Fan Noise, Technology and Numerical Methods (FAN2012)*, Senlis, France (CD-ROM, ISBN 978-0-9572374-1-4)